Crystal Structure of D-Hydantoinase from *Bacillus stearothermophilus*: Insight into the Stereochemistry of Enantioselectivity[†,‡]

Young-Hoon Cheon,[§] Hak-Sung Kim,[§] Kil-Hwan Han,[∥] Jan Abendroth,[⊥] Karsten Niefind,[⊥] Dietmar Schomburg,[⊥] Jimin Wang,*[,#] and Youngsoo Kim*[,∥]

Department of Biological Sciences, Korea Advanced Institute of Science and Technology, 373-1, Kusung-dong Yusung-gu, Taejon 305-701, Korea, School of Chemical Engineering, Yeungnam University, Dae-Dong, Kyungsan 712-749, Korea, Institut für Biochemie, Universität zu Köln, Zülpicher Strasse 47, 50674 Köln, Germany, and Department of Molecular Biophysics and Biochemistry, Yale University, 266 Whitney Avenue, New Haven, Connecticut 06520-8114

Received February 21, 2002; Revised Manuscript Received April 16, 2002

ABSTRACT: Industrial production of antibiotics, such as semisynthetic penicillins and cephalosporins, requires optically pure D-*p*-hydroxylphenylglycine and its derivatives as important side-chain precursors. To produce optically pure D-amino acids, microbial D-hydantoinase (E.C. 3.5.2.2) is used for stereospecific hydrolysis of chemically synthesized cyclic hydantoins. We report the apo-crystal structure of D-hydantoinase from *B. stearothermophilus* SD1 at 3.0 Å resolution. The structure has a classic TIM barrel fold. Despite an undetectable similarity in sequence, D-hydantoinase shares a striking structural similarity with the recently solved structure of dihydroorotase. A structural comparison of hydantoinase with dihydroorotase revealed that the catalytic chemistry is conserved, while the substrate recognition is not. This structure provides insight into the stereochemistry of enantioselectivity in hydrolysis and illustrates how the enzyme recognizes stereospecific exocyclic substituents and hydrolyzes hydantoins. It should also provide a rationale for further directed evolution of this enzyme for hydrolysis of new hydantoins with novel exocyclic substituents.

Microbial hydantoinase (HYD)[1] is an industrial enzyme (*1*). This enzyme has been used for the commercial production of optically pure D- or L-active amino acids in biocatalysis (*2*, *3*). It has also been used for the production of D-amino acid intermediate compounds through stereospecific hydrolysis of chemically synthesized cyclic hydantoins (*4*). These intermediates are widely used for semisynthetic antibiotics, peptide hormones, pyrethroids, and pesticides (*4*). Although the biology of microbial HYD remains largely unexploited and many natural substrates remain unknown, its homologous enzyme in humans is dihydropyrimidinase (DHP), which plays an essential role in the reductive pathway of pyrimidine degradation (*1*, *5*). It is essential for the detoxification of pyrimidine analogues that are used as pharmaceuticals, such as 5-fluorouracil (*6*). However, whether HYD and DHP are identical enzymes (see Scheme 1) remains unsettled (*7*−*9*), even though both have currently been assigned to the same enzyme classification (E.C. 3.5.2.2). There are also two members of the vertebrate neural specific collapsin-response-mediator protein gene family that share a substantial sequence similarity with HYD (*5*, *10*).

Scheme 1

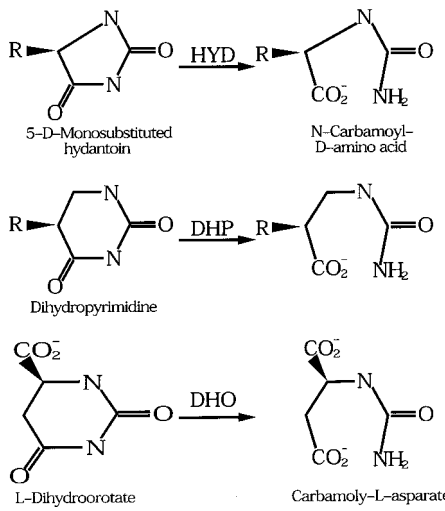

Hydantoinase was also subjected to directed evolution for enhanced stereochemical specificity and thermostability (*11*, *12*). Because of the potential commercial value of the structure-based design of the novel properties of these enzymes, both the L- and D-enantiomer specific hydantoinases were subjected to structural studies. A preliminary crystallographic analysis was also reported (*13*, *14*). In both cases, the asymmetric unit contained multiple copies of biologically active tetramers with the 222-particle symmetry, which made the structural determination quite challenging.

[†] J.W. acknowledges Yale University for start-up funds and thanks Dr. T. A. Steitz for financial support (NIH GM-22778). This work was supported by Grant RO2-2002-000-00013-0 from the Basic Research Program of the Korea Science and Engineering Foundation.

[‡] The refined coordinates have been deposited in the Protein Data Bank (http://www.rcsb.org/pdb/) with the accession number 1K1D.

* Correspondence should be addressed to either Y.K. (e-mail: ykim1@yu.ac.kr) or J.W. (email: wang@mail.csb.yale.edu).

[§] Korea Advanced Institute of Science and Technology.

[∥] Yeungnam University.

[⊥] Universität zu Köln.

[#] Yale University.

[1] Abbreviations: HYD, hydantoinase; DHO, dihydroorotase; DHP, dihydropyrimidinase; BstHYD, *Bacillus stearothermophilus* SD1 D-hydantoinase; TIM, triose phosphate isomerase; SGL, stereochemistry gate loop; aaHYD, *Arthrobacter aurescens* hydantoinase; NCS, noncrystallographic symmetry.

10.1021/bi0201567 CCC: $22.00
Published on Web 06/27/2002

Hydantoinase and dihydroorotase (DHO, see Scheme 1), as well as many other metallo-amidohydrolases, belong to a distantly related superfamily (*5*). Despite their lack of similarity in a one-dimensional sequence comparison, the structures of urease, phosphotriesterase, and adenosine deaminase belong to the classic triose phosphate isomerase (TIM) barrel fold and are similar (*5*). Homologous modeling by threading the sequences of HYD and DHO onto the known TIM barrel fold suggested that this superfamily included these two enzymes, whose structures were unknown (*5*). Both of these structures have now been determined.

In this report, we present the determination of the crystal structure of HYD, compare it with the recently determined structure of DHO (*15*), and discuss the stereochemistry of enantioselectivity.

EXPERIMENTAL PROCEDURES

Expression and Purification. The gene that encodes the full sequence of *Bacillus stearothermophilus* SD1 D-hydantoinase (BstHYD) (*16*) was inserted into the *Eco*R I and *Pst* I sites of the pMAL-c2 vector (New England BioLabs). The plasmid that bears the hydantoinase gene was transformed into *Escherichia coli* JM109 for protein expression. Following the manufacturer's recommended procedures (New England BioLabs), the induced hydantoinase was overexpressed and purified by affinity chromatography using amylose resin, and the tagging maltose-binding protein was removed by proteolytic digestion using factor Xa. The digested BstHYD carried four additional amino acids (Ile−Ser−Glu−Phe) at the N-terminus for introduction of the cleavage site of factor Xa. It was further purified by Sephadex G-200 gel-filtration chromatography (Pharmacia Biotech). Purified hydantoinase was concentrated to 10 mg/mL in a storage buffer (20 mM TrisCl, pH 7.5, 200 mM NaCl) for crystallization.

Crystallization and Data Collection. Within 3 days, the BstHYD crystals grew at 21 °C from hanging drops that contained 3 μL of the protein solution (10 mg ml^{-1} BstHYD, 20 mM Tris HCl, pH 7.5, and 200 mM NaCl) and 3 μL of the reservoir solution (100 mM TrisCl, pH 7.5, 2.1 M ammonium sulfate) by the vapor diffusion method against a 500 μL reservoir solution. The crystals were transferred to a cryosolution that contained 15%(w/v) glycerol and 3 M ammonium sulfate for 3 days before flash-cooling in a 100 K gaseous nitrogen stream. X-ray diffraction data were collected at the beamline 5.0.2 of the Advanced Light Source and the 6B MX beamline of the Pohang Accelerator Laboratory. The data were indexed and integrated using DENZO and scaled by SCALEPACK (*17*).

Computer Modeling of a Substrate−HYD Complex. The six-membered substrate L-dihydroorotate from its complex with DHO (*15*) was imported to our HYD structure using the least-squares superposition procedure that included all of the structurally equivalent Cα atoms that were defined by the DALI Program (*18*). A L-methionine residue with the most favorable rotamer conformation was manually placed onto L-dihydroorotate so that its side chain, including the Cα atom, would replace the two C atoms on the six-membered ring. After the replacement, a five-membered cyclic monosubstituted hydantoin with a L-methionine side chain was built as a substrate for HYD (the chirality is redefined to D once it is attached to the five-membered ring). The geometry (bond lengths, bond angles, and ring planarity) of this substrate was further idealized using the XPLO2D Program (*19*).

Table 1: X-Ray Data Collection and Refinement Statistics

Data Collection	
wavelength (Å)	0.91000
space group	C2
a (Å)	214.45
b (Å)	182.89
c (Å)	156.13
β (deg)	102.81
molecule/symmetric unit	8
V_m (Å^3/Da)	3.09
resolution (Å)	20−3.0
unique reflections	96,187
total observations	943,917
mosaicity (deg)	0.88
completeness (%)	99.9
R_{merge} (%, 3.0−3.1 Å)	13.8(64.2)
Refinement	
resolution (Å)	20−3.0
number of reflections used	91,758
number of test set reflections (10%)	9,138
R-factor (%, 3.0−3.2 Å)	26.3(40.1)
free R-factor (%, 3.0−3.2 Å)	28.0(43.1)
number of protein atoms	28,496
number of Zn ions	16
residues per subunit	1−460
missing residues per subunit	461−472
average *B* factor (Å^2)	53.6
rms *B* distribution (Å^2)	0.8
rms bond deviation (Å)	0.008
rms bond angle deviation (deg)	1.6
rms dihedral angle deviation (deg)	22.9
X-ray data/coordinates accession	1K1D

Sequence Alignment. Sequence alignment was carried out using the GCG's PILEUP Program (Wisconsin Genetic Computation Group, WI). The sequences that were used for the alignment include the following: *B. stearothermophilus* SD1 (BstSD, *16*), *B. stearothermophilus* NS1122A (BstNS, *20*), *Agrobacterium tumefaciens* (Agrot, *21*), human (*22*), rat (*23*), *Pseudomonas putida* (PseuP, *24*), and *Sinorhizobium meliloti* (Smeli, *25*).

Figures and Coordinates. Figures 2−6 were made using the Ribbons' Program (*26*). Coordinates were deposited in the RCSB Database (http://www.rcsb.org) under the accession number 1K1D.

RESULTS AND DISCUSSION

Patterson Analysis and Molecular Packing in Unit Cell. BstHYD crystals belong to the space group C2 with unit cell dimensions as follows: $a = 214.45$ Å, $b = 182.89$ Å, $c = 156.13$ Å, and $\beta = 125.27°$. The crystallographic asymmetric unit can accommodate 1, $1^1/_2$, 2, $2^1/_2$, and 3 copies of the tetrameric enzyme with corresponding Matthew's coefficients of 6.2, 4.1, 3.1, 2.5, and 2.1 Å^3/Da and a solvent content of 80%, 70%, 60%, 50%, and 40%, respectively. The self-rotation function and self-Patterson map calculations below show that there are two copies of tetramers per asymmetric unit. Other possibilities have been excluded. X-ray data collection statistics are summarized in Table 1.

A Patterson analysis showed that there were two tetramers in the asymmetric unit. The self-rotation function at $\kappa = 180°$

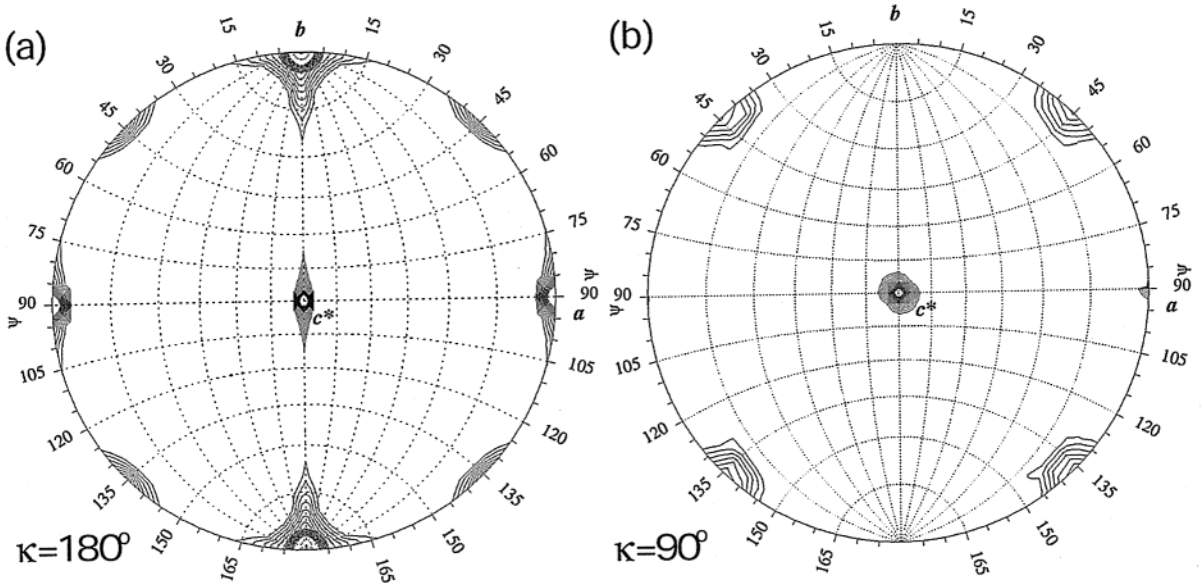

FIGURE 1: Self-rotation function in a standard orthogonalization convention with the *x* axis running parallel to the *a* axis, *y* axis to the *b* axis, and *z* axis to the *c** axis. (a) $\kappa = 180°$. The dyads of tetrameric particle 222 symmetry are oriented along diagonal axes between the *x* and *y* axes and the $-x$ and *y* axes, as well as along the *z* axis. Multiplication of particle's *z* axis dyad with the crystallographic (*y* axis) dyad results in a packing dyad along the *x* axis (Klug peak). The function was calculated using the data between 20 and 4.5 Å using the GLRF Program (*38*). (b) $\kappa = 90°$. An axis parallel with the tetrameric dyad along diagonal axes between the *x* and *y* axes (or the $-x$ and *y* axes) relates two tetramers by a rotation of 90°, resulting in a completely coincident set of 222 dyads. Multiplication of particle's diagonal dyads with the crystallographic dyad results in a packing 4-fold axis along the *z* axis in pseudo 422 symmetry. The function was calculated with the GLRF Program using the data between 20 and 5.0 Å.

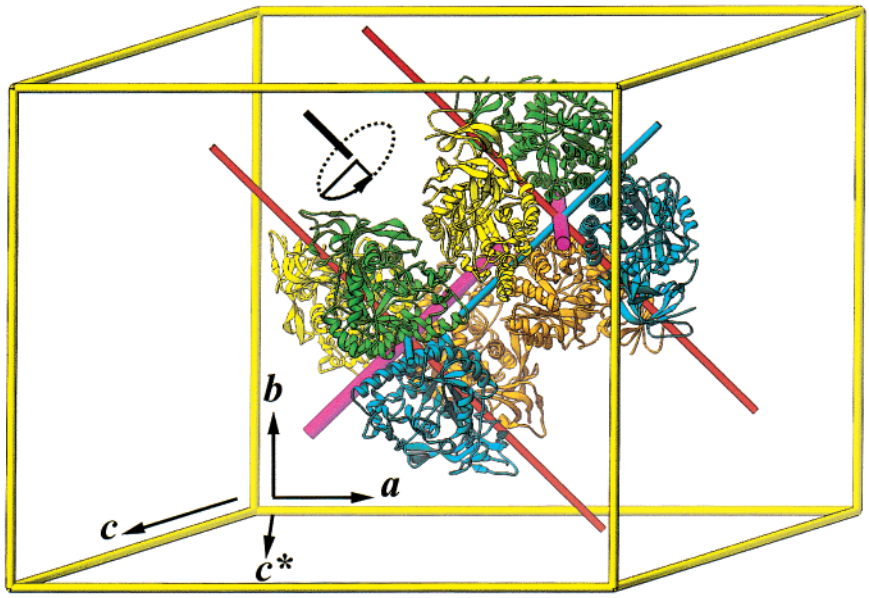

FIGURE 2: Packing of two tetramers in the crystallographic asymmetric unit within one unit cell, viewing approximately down the *z* axis dyad. Dyads are shown as red, magenta, and cyan sticks. Note a 90° rotation axis parallel to the red axes that relates the two tetramers.

showed that there was a complete set of 222-particle symmetry peaks with one dyad that was parallel to the *z* axis. The other two dyads were diagonal to the *x* and *y* axes within the *xy* plane (Figure 1a). Multiplication of one particle dyad at the *z* axis with the crystallographic dyad at the *y* axis (*b* axis) resulted in a Klug peak (or packing symmetry) at the *a* axis. Therefore, there was at least one particle with dyads that were oriented the same as these peaks. Two identical tetramers may share one set of 222 symmetry peaks in self-rotation functions in the following two cases. In the first case, two particles are related by a translation vector, the possibility of which had been excluded because of the lack of pseudo-origin peaks in the self-Patterson (native Patterson map) calculations. In the second case, two particles are related by a rotation of 90° along an axis that is parallel to one of the particle 222 dyads. This case is clearly possible in the self-rotation map calculations at $\kappa = 90°$ (Figure 1b). If we choose this rotational axis in the first symmetric unit that is diagonal to the *x* axis and *y* axis with the *xy* plane (Figure 2), then the packing symmetry operations will generate rotations of 90° around the two additional axes that are parallel to the two other 222-particle dyads (Figure 1b).

This packing information is critical in the interpretation of rotation functions from the molecular replacement in which the correct solutions were buried below the noise levels.

The lack of pseudo-origin peaks in the self-Patterson map calculation has also excluded other possibilities, such as half tetramers or a third tetramer in the asymmetric unit. Whether there are $1^1/_2$ or $2^1/_2$ tetramers in the asymmetric unit, one tetramer must sit on the crystallographic dyad with the other two dyads that are parallel with the *x* axis and *z* axis. In this case, there should be a pseudo-origin peak in the self-Patterson calculations. Similarly, if there is a third tetramer with its 222 dyads, this tetramer has to be oriented as one of the two other tetramers that were described previously. There should also be a pseudo-origin peak. The absence of such peaks has excluded these possibilities.

Structural Determination. After the Patterson analysis, the structural determination included molecular replacement, noncrystallographic symmetry (NCS) averaging, and structural refinement. The initial structural determination included a molecular replacement using both programs, CNS (*27*) and CCP4's AMoRe (*28*, *29*), with the tetrameric coordinates of hydantoinase from *Thermus* sp., a closely related species (*14*). The correct solutions (found in retrospective examinations), however, were all below noise levels. The top translation solutions (one per rotation) that were possible in the one-tetramer search model were systematically duplicated in order to generate two-tetramer models. One tetramer was fixed in place. The second tetramer was rotated using rotational matrixes that were derived from self-rotation functions, described previously in the Patterson analysis. The lowest *R*-factor for all of the possible two-tetramer model solutions (using data between 15 and 4.0 Å) was 52%. However, these solutions failed to refine them further. Fortunately, one solution was sufficiently accurate for generating NCS matrixes and the initial mask for "ab initio" NCS averaging (*30*, *31*). The result was averaged maps that were sufficient to allow the development of a complete model with a correct sequence. These maps also clearly showed carbamated K150 and two bound metal ions at the hydrolysis active sites in each subunit. The identity of these metal ions is still unknown. They are tentatively assigned as zinc. Additional attempts of maskless averaging were made to improve the maps for 16 residues at the C-terminus, including 4 residues that were added at the N terminus as the result of the construct (see above). The atomic model was refined using a standard refinement procedure that used noncrystallographic symmetry restraints. The final model included residues 1−460 with two zinc ions per subunit. Refinement statistics are summarized in Table 1.

The structural determination was challenging, even after we incorporated the Patterson analysis results and applied noncrystallographic symmetry (NCS). We wanted to understand why, so we continued our search. We found that the tetrameric models of *Thermus* sp. (*14*) and BstHYD had slightly different oligomeric structures. There is an overall difference of 4.5 Å among the Cα coordinates of the two tetrameric enzymes. There is a 56% difference in the amino acids between *Thermus* sp. and BstHYD. This caused one dimeric interface to expand by 1.9 Å and the second dimeric interface by 3.6 Å.

Overall Structure of D-hydantoinase. BstHYD crystallizes as a biologically active tetramer. It has an olive shape with

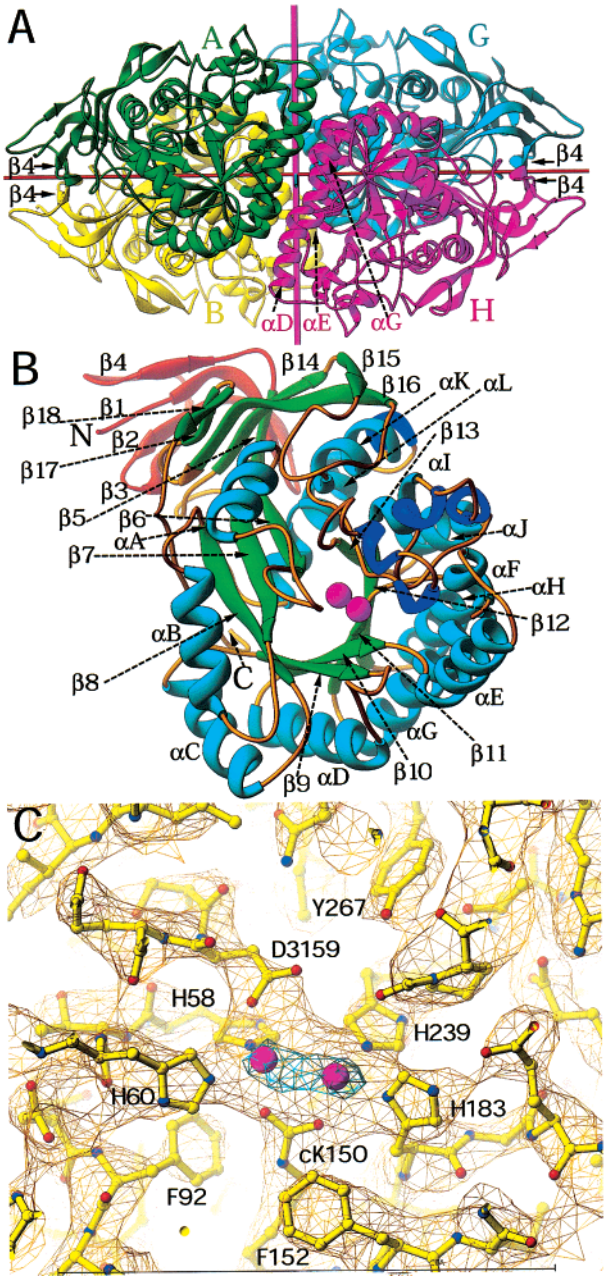

FIGURE 3: Overall structure of hydantoinase. (A) Tetramer. Key secondary structural features at subunit interfaces are indicated. (B) Monomer with the hydrolytic active site is marked with two bound zinc ions (magenta spheres). Secondary structures are as follows: *β*1(6−11), *β*2(16−23), *β*3(27−32), *β*4(42−44), *β*5(49−52), *β*6-(54−58), αA(74−83), *β*7(86−93), αB(101−112), *β*8(119−125), αC(131−142), *β*9(148−152), αD(163−176), *β*10(179−183), αE-(187−199), αF(206−210), αG(214−231), *β*11(234−237), αH-(243−254), *β*12(258−263), αI(265−269), αJ(296−306), *β*13(310−312), αK(345−352), αL(361−375), *β*14(393−398), *β*15(401−403), *β*16(422−432), *β*17(437−439), and *β*18(442−444). (C) A portion of the composite-omit electron density map at the hydrolysis active site at 1.0*σ* (golden) and 5.0*σ* (cyan) with two bound zinc ions (magenta spheres). Active site residues, including carbamated lysine (cK150), are labeled.

dimensions of 125 × 81 × 72 Å^3. There are two distinct sets of subunit interfaces in the tetramer. One is dominated by an extended eight-stranded *β*-sheet with four strands from each subunit (subunits A and B in Figure 3a); the second is dominated by coiled−coil interactions with three α-helices from each subunit (subunits A and H in Figure 3a). Each interface buries a substantial solvent-accessible surface (*32*)

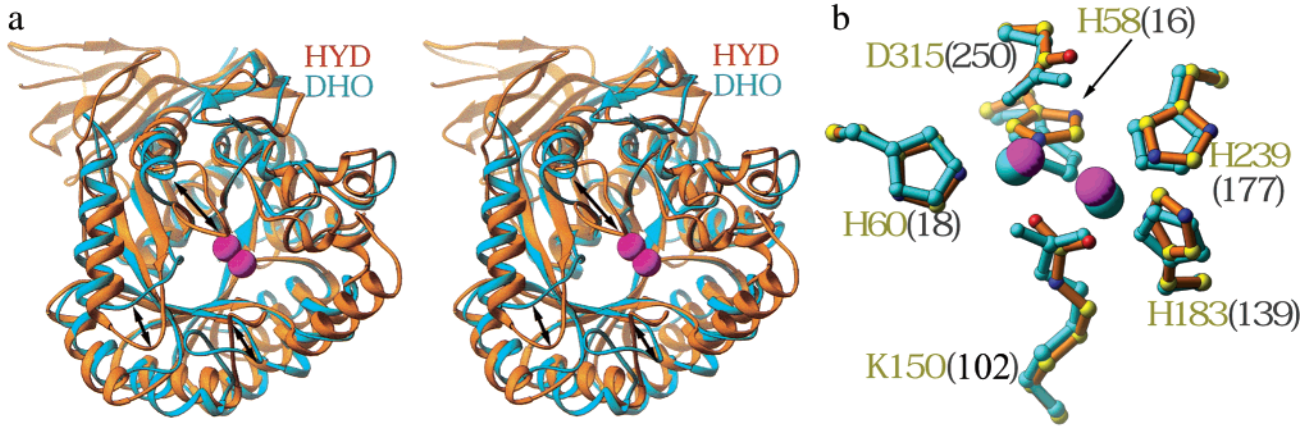

FIGURE 4: Structural similarity between hydantoinase (HYD) and dihydroorotase (*15*). Spheres represent two bound zinc ions: magenta for HYD and cyan for DHO. (a) The overall superposition of HYD (brown) and DHO (cyan). (b) A close-up of the active site with HYD active-site residues (brown) and DHO (cyan).

with 2200 and 2100 Å^2 for the first and second sets, respectively. The BstHYD subunit structure has a more globular shape with dimensions of 42 × 52 × 62 Å^3. Each subunit has a complete hydrolytic active site that is marked by two zinc ions (Figure 3b,c). The hydrolytic active sites in the tetramer are nicely separated by at least 40 Å.

Hydantoinase Has a Classic TIM Barrel Fold. The BstHYD subunit has a classic TIM barrel fold and an extra domain (Figure 3b). A pairwise comparison with known structures in the protein database using the DALI Program (*33*) revealed that the BstHYD TIM barrel core shared a striking homology with four other structures. They were as follows: DHO (*15*), urease (*34*), phosphotriesterase (*35*), and adenosine deaminase (*36*) with structural similarity *z*-scores (which are proportional to similarity; the higher the score, the more the similarity) of 32.3, 22.9, 18.0, and 15.1, respectively. The BstHYD coordinates differed from DHO (the structure with the most similarity) by a rms deviation of 2.7 Å for 318 common Cα atoms, as defined by the DALI alignment, even though these two enzymes shared only a 16% sequence identity and a 25% sequence similarity.

Structural Similarities between Hydantoinase and Dihydroorotase. BstHYDs use similar coiled−coil interactions for dimerization (Figure 3a) as DHO (*15*). Unlike the dimeric DHO (*15*), the dimeric BstHYDs are dimerized further to form a tetramer, using the N-terminal β-sheet from its extra domain. This domain includes the N- and C-termini (β1 to β4 and β14 to β18; Figure 3b). Oligomerization may be important for allosteric regulation, which is a property of these enzymes. For example, in the crystal structure of dimeric DHO, one subunit was observed to bind the substrate and the other to bind the product (*15*), suggesting cooperate action between the two subunits. Such mixed states may also be important in HYD because its hydrolytic active site is completely buried (see below). Both the substrate binding and product release would require transient opening of the active sites.

Structural similarities between BstHYD and DHO further extend to active sites, implying a conserved hydrolytic mechanism through divergent evolution. The DHO active site for hydrolysis, which includes two zinc ions and their ligands, four histidines, one aspartate, and one carbamated lysine, can be superimposed onto the equivalent zinc ions and protein ligands of HYD using the DALI-defined structural alignment (Figure 4). This structural alignment defines the hydrolytic active site in BstHYD.

Structural similarity shows that both BstHYD and DHO are more similar to each other than to any other protein structure that is found in the DALI database. This leads us to suggest that BstHYD and DHO belong to a di-zinc metalloenzyme small subfamily within a large distantly related amidohydrolase superfamily, which shares a conserved binuclear metal ion catalytic mechanism. In the mechanism, one metal ion activates an attacking hydroxyl, and the second metal ion stabilizes the oxyanion intermediate (*15*). Consistent with our suggestion, previous biochemical data have shown that DHO is a metalloenzyme (*37*), even though the metal identity was not explicitly established. Interestingly, the structural similarity between HYD and DHO was previously predicted upon threading the sequences onto known structures of adenosine deaminase (a one-zinc enzyme) (*36*), urease (a bi-nickel enzyme) (*34*), and phosphotriesterase (a bi-cadmium enzyme) (*35*). Our findings confirmed their prediction. We show the extraordinary power of the three-dimensional structures in revealing similarities that are not evident from the sequence comparisons (*5*).

Inferred Mode of Substrate Binding. The crystal structure of BstHYD allows a binding site for the cyclic substrate 5-D-monosubstituted hydantoin (Figure 5) to be identified on the basis of modeling, using the structure of the DHO−dihydroorotate complex (*15*). The inferred binding site consists of recognition sites for the functional amino groups and exocyclic substituents of hydantoins. The recognition of the functional amide groups (CO−NH−CO−NH on the substrate ring arranged counterclockwise in Scheme 1 and Figure 5, view from the top of the TIM barrel) controls the ring orientation of the bound substrate, while the recognition of the exocyclic substituents determines the stereochemistry of the hydrolysis products. In the DHO−dihydroorotate complex (*15*), the orientation of the cyclic amino derivative is precisely defined through a network of hydrogen bonds with functional groups on its ring. The ring-opening hydrolysis occurs in the first of the two consecutive amide bonds (CO···NH−CO−NH, see Scheme 1). These functional amide groups form hydrogen bonds sequentially with the following ligands (Figure 5a): (i) zinc ions, (ii) the attacking hydroxyl (not shown in Figure 5a), (iii) the backbone carbonyl and amine of L222 (followed by a conserved *cis*-

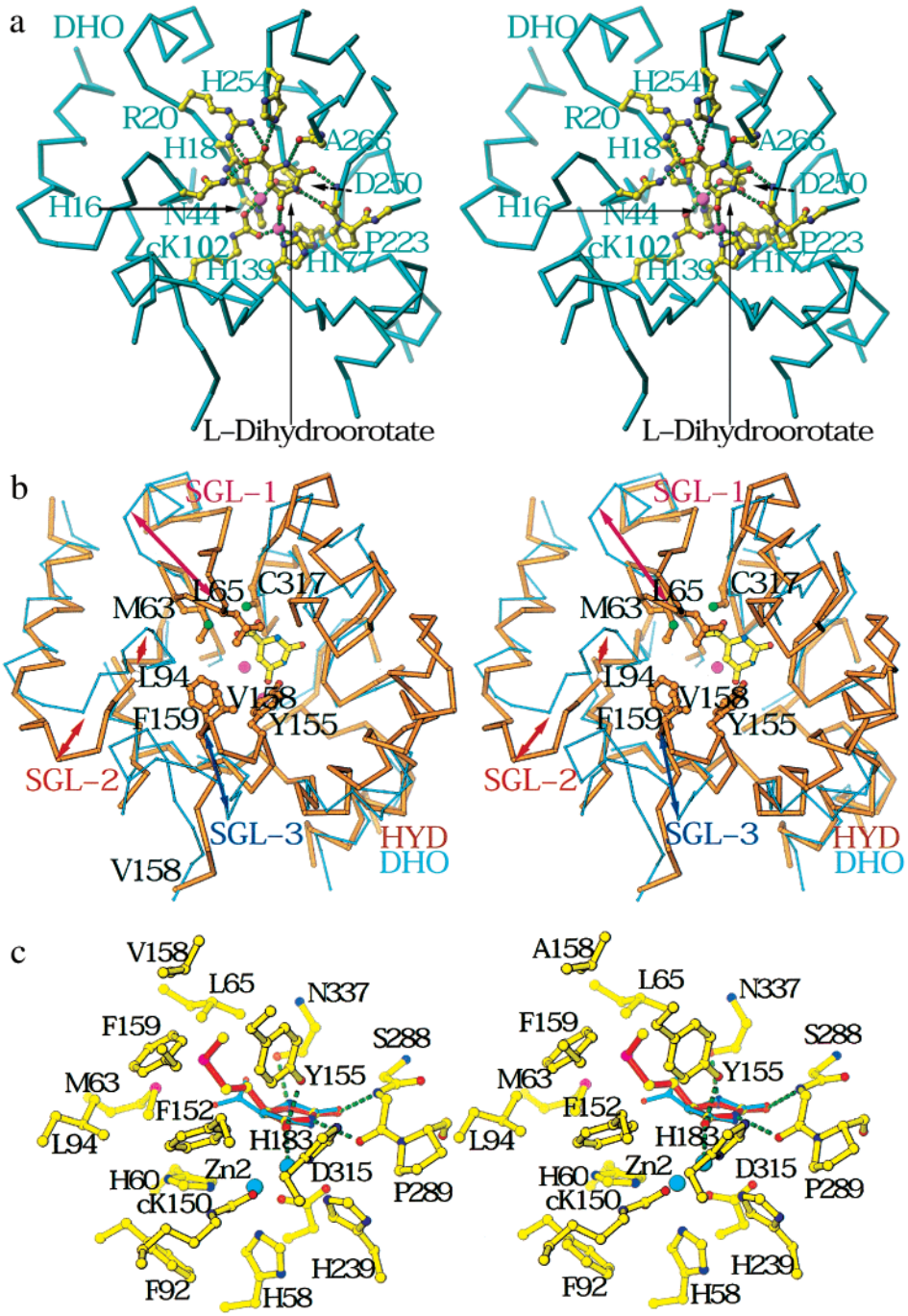

FIGURE 5: Substrate binding sites in DHO and HYD. (a) The binding of L-dihydroorotate to DHO (*15*). (b) To identify the substrate-binding site in HYD, we imported bound L-dihydroorotate (yellow) with DHO (thin cyan sticks) from panel a onto HYD (thick brown sticks). Three stereochemistry gate loops (SGL) are indicated where two structures differ substantially near the substrate binding pockets. L65, Y155, V158, and F159 make a part of the lid for (and to seal off) the substrate-binding pocket. Double-ended arrows indicate large structural differences between HYD and DHO in SGL-1, SGL-2, and SGL-3. The L94 Cα atom is shown as a white circle (see text for discussion). (c) A close-up stereodiagram of HYD with modeled L-methionine-substituted hydantoin (red) and L-dihydroorotate (cyan). Hydrogen bonds are represented in green dashes.

peptide proline between the two enzymes), and (iv) the backbone carbonyl of A266. Their equivalent residues in BstHYD are S288 (followed by *cis*-peptide P289) and N337, respectively (Figure 5c). One would predict that each enzyme binds and hydrolyzes its respective substrates in an identical manner since the ligands that make these interactions in DHO (*15*) are backbone atoms that are located in the conserved TIM barrel.

A modeled substrate (the monosubstituted hydantoin with a methionine side chain) fitted nicely into our HYD structure with no physical overlap (Figure 5c). The functional groups are recognized by HYD in a manner identical to that expected from the DHO−dihydroorotate complex (*15*). BstHYD and DHO, however, recognize different exocyclic substituents on the cyclic amine substrates. DHO recognizes an exocyclic carboxylate (*15*), whereas HYD recognizes side chains of the amino acids. Nevertheless, substituents of both substrates point in the same direction to the chiral center (Figure 5c, Scheme 1). Therefore, the approximate location of substituents in BstHYD can be inferred from the DHO structure

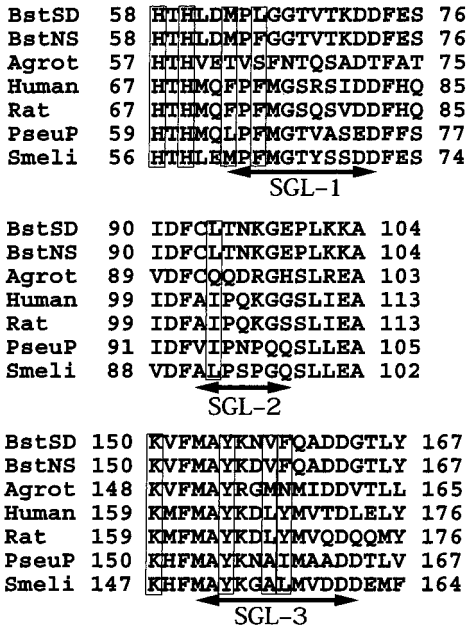

FIGURE 6: Sequence alignment at three stereochemistry-gate loops near the substrate-binding pocket and hydrolysis active site. Ligands for zinc ions are boxed (H58, H60, and K150), and so are the key features that make the lid of the substrate-binding pocket.

(*15*). In DHO (*15*), the recognition of the exocyclic carboxylate of L-dihydroorotate, which is exposed in the binding pocket (Figure 5a, 5b), is accomplished by hydrogen bonds with the enzyme side chains of N44, R20, and H254. In HYD, the recognition of the exocyclic side chain of 5-D-monosubstituted hydantoin is at an equivalent location with respect to DHO (*15*), but in a completely buried hydrophobic pocket (Figure 5b,c). The residues that form the pocket include M63, L65, F152, F159, and Y155 from three loops (stereochemistry gate loops or SGL). The hydrophobic nature of this pocket implies that this enzyme works only for hydrophobic amino acid residues on hydantoins, but not charged residues. These loops, SGL-1 (residues 62−72), SGL-2 (residues 93−100), and SGL-3 (residues 153−162), are highly conserved among the D-HYD sequences (Figure 6). The Y155 side chain, which is absolutely conserved in HYD (Figure 6), forms a hydrogen bond with the functional group where hydrolytic chemistry takes place.

The stereochemistry gate loops may account for the substrate specificity in HYD and DHO. The conformations of these loops differ substantially between the two enzymes (Figure 5b). The largest Cα coordinate displacement in each loop is 15.3, 14, and 9.4 Å between BstHYD and DHO, respectively. With respect to DHO (*15*), SGL-2 in BstHYD is displaced away from the binding pocket. SGL-1 and SGL-3 are shifted into and make up a part of the lid of the substrate-binding pocket. The side chain of L65 in SGL-1, and those of Y155, V158, and F159 in SGL-3 in BstHYD, completely sealed the binding pocket (Figure 5b). These conformational differences also make the buried substrate-binding site smaller in BstHYD than that in DHO. In the modeling (Figure 5c), the carboxylate of the imported six-membered cyclic L-dihydroorotate appears to be too close to the backbone of N337 of HYD, while the modeled five-membered cyclic substrate forms a nearly perfect hydrogen bond. This difference explains why BstHYD recognizes a five-membered ring in hydantoins, while DHO recognizes a six-membered ring.

Structural Basis for the Stereochemistry of Enantioselectivity. Structural determinants for the chiral exocyclic substituent of the substrate provide insight on the stereochemistry of enantioselectivity in HYD and DHO. In both the L-dihydroorotate (substrate for DHO) and 5-D-monosubstituted hydantoin (substrate for HYD), the exocyclic substituents point toward the viewer in Scheme 1. The chiral proton points into the protein core where a large substituent (as in inverted enantioselectivity) is not permitted because of the potential overlap with the following structural elements (Figures 4b and 5a,b): (i) side chains of the catalytic ligands of aspartate (D315 in HYD and D250 in DHO) and histidine (H60 in HYD and H18 in DHO), (ii) bound zinc ion, and (iii) the side chain of an additional residue (C317 in HYD and A252 in DHO) that is adjacent to the aspartates. These features can account for the recognition of D-enantiomeric hydantoins by HYD and L-enantiomeric hydroorotate by DHO.

The *Arthrobacter aurescens* hydantoinase (aaHYD) has some unusual properties in regard to the stereospecific hydrolysis of hydantoins (*4*). *A. aurescens* is one of the few microorganisms that produces L-HYD, which converts 5-monosubstituted hydantoins into L-amino acids in catalysis (*4*), while most of the other microorganisms produce D-enantiomers. When aaHYD is used for the production of methionine, it behaves like normal D-HYD and produces more D-enantiomer than L-enantiomer (*4*, *11*). Surprisingly, a single mutation (I95L) that is derived from the directed evolution inverted enantioselectivity to more than 99% of L-enantiomer (*11*). According to the sequence similarity, aaHYD is related to the other D-hydantoinases. For example, HYDs from *A. aurescens* and *B. stearothermophilus* SD1 share a 35% identity and a 44% similarity in sequence. The catalytic ligands of BstHYD are present in aaHYD, which implies that there is a conserved hydrolytic mechanism. However, there is very little recognizable similarity with the gaps and insertions in three SGLs. Interestingly, the key residue (I95L) that controls the enantioselectivity inversion mutation in aaHYD is located in SGL-2 at an equivalent residue of L94 in BstHYD (Figure 5b, 5c). This residue is about 5.6 Å away from the modeled substrate (Figure 5c). This suggests two possibilities: one is a different recognition pocket, and the other is an indirect effect of recognition in that enzyme. Interestingly, its equivalent residue in DHO is N44 (Figure 5a), also a determinant element for the recognition of the exocyclic carboxylate substituent in the DHO−hydroorotate complex (*15*). Therefore, the identification of the three SGLs should open a new avenue to directed evolution in this enzyme for the hydrolysis of new hydantoins with novel exocyclic substituents.

ACKNOWLEDGMENT

We would like to thank Drs. W. H. Konigsberg and W. P. Kennedy for critically reading this manuscript. H.K. thanks Dr. Oliver May for his helpful discussion. Y.K. thanks Drs. Thomas Earnest and Jerry McDermott for assistance on the ALS 5.0.2 beamline and Drs. H. S. Lee, K. H. Kim, and S. S. Cha for assistance on the 6B MX beamline of the Pohang Accelerator Laboratory.

REFERENCES

1. Syldatk, C., May, C. O., Altenbuchner, J., Mattes, R., and Siemann, M. (1999) *Appl. Microbiol. Biotechnol. 51*, 293−309.
2. Park, J. H., Kim, G. H., and Kim, H. S. (2000) *Biotechnol. Prog. 16*, 564−570.
3. Wilms, B., Wiese, A., Syldatk, C., Mattes, R., and Altenbuchner, J. (2001) *J. Biotechnol. 86*, 19−30.
4. Ogawa, J., and Shimizu, S. (2001) *Trends Biotechnol. 17*, 13−20.
5. Holm, L., and Sander, C. (1997) *Proteins: Struct., Funct., Genet. 28*, 72−82.
6. Naguib, F. N., el Kouni, M. N., and Cha, S. (1985) *Cancer Res. 45*, 5405−5412.
7. Runser, S., and Meyer, P. C. (1993) *Eur. J. Biochem. 213*, 1315−1324.
8. Ogawa, J., and Shimizu, S. (1997) *J. Mol. Catal. B 2*, 163−176.
9. Ogawa, J., Honda, M., Soong, C. L., and Shimizu, S. (1995) *Biosci. Biotechnol. Biochem. 59*, 1960−1962.
10. Takemoto, T., Sasaki, Y., Hamafima, N., Goshima, Y., Nonaka, M., and Kimura, H. (2000) *Gene 261*, 259−267.
11. May, O., Nguyen, P. T., and Arnold, F. H. (2000) *Nat. Biotechnol. 18*, 317−250.
12. Kim, G. J., Cheon, Y. H., and Kim, H. S. (2000) *Biotechnol. Bioeng. 68*, 211−217.
13. May, O., Siemann, M., Syldatk, C., Niefind, K., and Schomburg, D. (1996) *Acta Crystallogr, Sect. D52*, 1209−1210.
14. Abendroth, J., Niefind, K., Chatterjee, S., and Schomberg, D. (2000) *Acta Crystallogr., Sect. D56*, 1166−1169.
15. Thoden, J. B., Philips, J., G. N., Neal, T. M., Raushel, F. M., and Holden, H. M. (2001) *Biochemistry 40*, 6989−6997.
16. Kim, G. J., Park, J. H., Lee, D. C., Ro, H. S., and Kim, H. S. (1997) *Mol. Gen. Genet. 255*, 152−156.
17. Otwinowski, Z., and Minor, W. (1997) *Methods Enzymol. 276*, 307−326.
18. Holm, L., and Lander, C. (1993) *J. Mol. Biol. 233*, 123−138.
19. Kleywegt, G. J., and Jones, T. A. (1997) *Methods Enzymol. 277*, 208−230.
20. Mukohara, Y., Ishikawa, T., Watabe, K., and Nakamura, H. (1994) *Biosci. Biotechnol. Biochem. 58*, 1621−1626.
21. Grifantini, R., Galli, G., Carpani, G., Pratesi, C., Frascotti, G., and Grandi, G. (1998) *Microboilogy 144*, 947−954.
22. Hamajima, N., Matsuda, K., Sakata, S., Tamaki, N., Sasaki, M., and Monaka, M. (1996) *Gene 180*.
23. Matsuda, K., Sakata, S., Kaneko, M., Hamajima, N., Nonaka, M., Sasaki, M., and Tamaki, N. (1996) *Biochim. Biophys. Acta 1307*, 140−144.
24. Chien, H. R., Jih, Y. L., Yang, W. Y., and Hsu, W. H. (1998) *Biochim. Biophys. Acta 1395*, 68−77.
25. Capela, D., Barloy-Hubler, F., Gouzy, J., Bothe, G., Apme, F., Batut, J., Boistard, P., Becker, A., Boutry, M., Cadieu, E., Dreano, S., Gloux, S., Godrie, T., Goffeau, A., Kanh, D., Kiss, E., Selaure, V., Masuy, D., Pohl, T., Portetelle, D., Puhler, A., Purnelle, B., Ramsperger, U., Renard, C., Thebault, P., Vandenbol, M., Weidner, S., and Galibert, F. (2001) *Proc. Natl. Acad. Sci. U.S.A. 98*, 9877−9882.
26. Carson, M. (1991) *J. Appl. Crystallogr. 24*, 958−961.
27. Brunger, A. T., Adam, P. D., Clore, G. M., DeLano, W. L., Gros, P., Gross-Kunstelve, R. W., Jiang, J. S., Kuszewski, J., Nilges, M., Pannu, N. S., Read, R. J., Rice, L. M., Simonson, T., and Warren, G. L. (1998) *Acta Crystallogr., Sect. D 50*, 905−921.
28. Combined Computational Project4 (1994) *Acta Crystallogr., Sect. D 50*, 760−763.
29. Navaza, J. (1994) *Acta Crystallogr., Sect. A 50*, 157−163.
30. Wang, J., Hartling, J. A., and Flanagan, J. M. (1997) *Cell 91*, 447−456.
31. Wang, J., Hartling, J. A., and Flanagna, J. M. (1998) *J. Struct. Biol. 124*, 151−163.
32. Richards, F. M. (1997) *Annu. Rev. Biophys. Bioeng. 6*, 151−176.
33. Holm, L., and Sander, C. (1993) *J. Mol. Biol. 233*, 123−138.
34. Benini, S., Ryniewski, W. R., Wioson, K. S., Ciurli, S., and Mangani, S. (1998) *J. Biol. Inorg. Chem. 3*, 268−273.
35. Benning, M. M., Kuo, J. M., Raushel, F. M., and Holden, H. (1995) *Biochemistry 34*, 7973−7978.
36. Wang, Z., and Quiocho, F. A. (1998) *Biochemistry 37*, 8314−8324.
37. Williams, N. K., Manthey, M. K., Hambley, T. W., O'Donoghue, S. I., Keegan, M., Chapman, B. E., and Christopherson, R. I. (1995) *Biochemistry 34*, 11344−11352.
38. Tong, L., and Rossmann, M. G. (1997) *Methods Enzymol. 276*, 594−611.

BI0201567